Noname manuscript No.
(will be inserted by the editor)

Stopping waves: Geometric analysis of coupled bursters in an asymmetric excitation field

Iulia Martina Bulai · Morten Gram Pedersen

Received: date / Accepted: date

Abstract Bursting is a type of electrical activity seen in many neurons and endocrine cells where episodes of action potential firing are interspersed by silent phases. Here we investigate partial synchrony and wave propagation in a population of square-wave bursters. In particular, by using a prototypical polynomial bursting model and slow/fast bifurcation analysis, we study why electrically coupled model bursters typically synchronize very easily, as reflected in the tendency for simulated excitation waves to propagate far into the region of silent cells when an excitation gradient is imposed. Such simulation are inspired by, but do not reproduce, experimentally observed Ca^{2+} waves in pancreatic islets exposed to a glucose gradient. Our analyses indicate a possible modification of the model so that the excitation waves stop at the border between "active" and "silent" cells. We verify this property by simulations using such a modified model for a chain, and for a cubic cluster, of coupled cells. Furthermore, we show how our one- and two-parameter bifurcation analyses allow us to predict where the simulated waves stop, for both the original model and the modified version.

Keywords Bursting electrical activity · Wave block · Slow/fast analysis · Cell population

PACS 34C23 · 34C60 · 37N25 · 70K70 · 92C37

I. M. Bulai (corresponding author)
Department of Information Engineering, University of Padova. Via Gradenigo, 6/B, 35131, Padova, Italy. Member of the research group GNCS of INdAM.
Tel.: +39-0498277758. E-mail: bulai@dei.unipd.it, ORCID 0000-0002-9570-8532

M. G. Pedersen
Department of Information Engineering, and Department of Mathematics "Tullio Levi-Civita", University of Padova. Via Gradenigo, 6/B, 35131, Padova, Italy.
Tel.: +39-0498277961. E-mail: pedersen@dei.unipd.it, ORCID 0000-0002-2639-2394

1 Introduction

Synchronization and desynchronization of electrically active cells is of biological interest, for example for our understanding of neuronal activity, cardiac function and pulsatile hormone release. Such synchronization may come about because of wave propagation across the cell population due to, e.g., electrical coupling via gap junctions [2, 5, 6].

Many cells exhibit bursting electrical activity where episodes of action potential firing (active phases) are interspersed by silent phases of quiescence. Many biophysical [10, 12, 37] and purely mathematical, e.g. polynomial [17, 29], models of bursting oscillators (bursters) have been proposed. The latter ones have the advantage of being analytically tractable. For example, a thorough bifurcation analysis can be performed [15, 17, 27, 35].

A prototypical example of so-called square-wave bursters consists of pancreatic β-cells [34]. The β-cells are electrically coupled in the pancreatic islets, microorgans forming the endocrine pancreas, and excitation waves have been observed to propagate across the islets using dyes sensitive to Ca^{2+} [2, 4, 16, 33, 36] or voltage [16]. These waves were initially suggested to be a means for active β-cells to recruit otherwise silent cells to release insulin [2]. However, subsequent studies showed that when an islet is subjected to a glucose gradient so that a part of the β-cell population of the islet is exposed to glucose levels above the threshold for activation, whereas the other part of the islet is experiencing glucose concentrations below this threshold level, wave propagation is observed only in the part of the islet where glucose is above the activation threshold, and does not propagate into the "silent" region of the islet [5, 33].

Mathematical modeling has been successfully used to study various aspects of β-cell function in mice [7, 23] and humans [24, 32], including the role of gap junction coupling in wave propagation [2, 4, 20, 22]. However, simulations of current mathematical models of electrical activity in β-cells are unable to reproduce the experimental fact that, in the presence of a glucose gradient, excitation wave do not propagate into the region of the islets with below-activation levels of glucose [5, 33]. Further, modeled β-cells tend to synchronize much more easily than experimentally observed. To improve the simulation results, unrealistically low coupling strength [11, 25], exaggerated cell-to-cell heterogeneity [19], or a particular isles-within-islets structure [3] have been assumed.

Inspired by the partial synchrony observed experimentally in β-cells [5, 33], in this paper we analyze why square-wave bursters tend to activate very easily when coupled to an active neighbor, which underlies the fact that simulated waves propagate into the region of cells that would be silent when uncoupled. We study a generic mathematical model [27, 29] with techniques from slow/fast bifurcation analysis. Our analysis suggest a possible modification of the model to obtain waves that do not propagate into the "silent" region of the islets. We confirm this prediction by performing simulations where single cells are represented by such a modified model, and the cells are coupled with biologically realistic coupling strengths. Our work does not investigate the role

of gap junction coupling in modifying the burst period and the underlying bifurcation structure, which has been studied elsewhere [13–15, 18, 21].

2 A polynomial bursting model

A prototypical mathematical model describing the electrical activity of N coupled bursting cells on a line in nondimensionalized form is [28, 30] (here and in the following over-dots indicate time derivatives)

$$\begin{aligned} \dot{u}_i &= f(u_i) - w_i - g(c_i) + g_c(u_{i-1} - 2u_i + u_{i+1}), \\ \dot{w}_i &= \frac{w_\infty(u_i) - w_i}{\tau_w(u_i)}, \\ \dot{c}_i &= \epsilon H(u_i, c_i), \end{aligned} \tag{1}$$

where $i = 1, ..., N$, counts the cells, ϵ is a constant such that $0 \leq \epsilon \ll 1$, while the functions $f(u_i)$, $g(c_i)$, $w_\infty(u_i)$, $\tau_w(u_i)$ and $H(u_i, c_i)$ have biological interpretations related to the different ionic currents and their kinetics. The first equation describes the temporal behavior of the transformed membrane potential u_i of the ith cell, which is electrically coupled to its neighbors as described by the last term, where g_c represent a constant nondimensionalized gap junction conductance, which we assume equal between all cells. We assume no-flux boundary conditions, which corresponds to setting (formally) $u_0 = u_1$ and $u_{N+1} = u_N$. Finally, w_i and c_i are variables controlling fast and slow ion channel gating, respectively.

By differentiating (1) in t and combining the first two equations of the model to eliminate w_i [27–30], we get the following system for u_i and c_i,

$$\begin{aligned} \ddot{u}_i + [F(u_i) + 2g_c]\,\dot{u}_i + [G(u_i, c_i) + 2g_c u_i] & \\ -g_c(u_{i+1} + u_{i-1} + \dot{u}_{i+1} + \dot{u}_{i-1}) &= -\epsilon H(u_i, c_i), \\ \dot{c}_i &= \epsilon H(u_i, c_i), \end{aligned} \tag{2}$$

where [27, 29]

$$\begin{aligned} F(u_i) &= a\left[(u_i - \hat{u})^2 - \eta^2\right], \\ G(u_i, c_i) &= c_i + u_i^3 - 3(u_i + 1), \\ H(u_i, c_i) &= \beta\left[u_i - (\bar{u} - b_i)\right] - c_i, \end{aligned} \tag{3}$$

are, respectively, second, third and first order polynomials in u_i. The parameters b_i control how active the cells are if uncoupled, and would in the case of β-cells reflect the glucose concentration sensed by cell i. We can therefore model a glucose gradient by letting $i \mapsto b_i$ be a monotone function of i.

Fig. 1 (top panel) shows a simulation of this scenario with a chain of 100 uncoupled cells ($g_c = 0$) and a linear relation $b_i = 0.012 \cdot i$. Note that activity decreases with increasing b_i, and that the last active cell is for $i = 24$. We then performed simulations with $g_c = 0.1$, which is equivalent to a

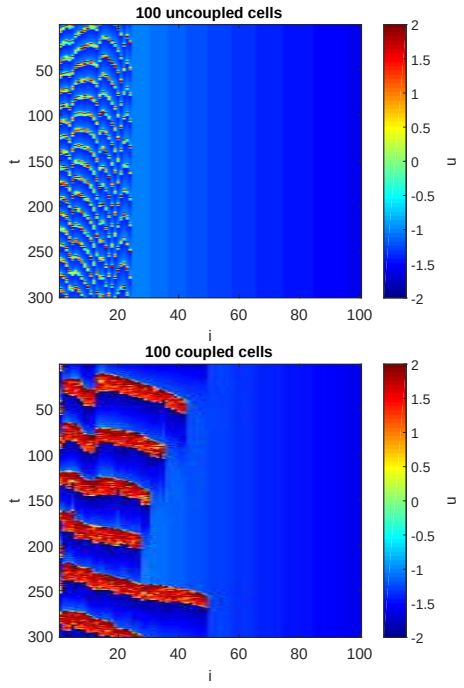

Fig. 1: Waves propagate into the silent region with the Pernarowski model. Color-coded transformed membrane potentials u_i for 100 uncoupled (top, $g_c = 0$) or coupled (bottom, $g_c = 0.1$) cells in an excitation gradient ($b_i = 0.012 \cdot i$). The last active cell is, respectively, $i = 24$ and $i = 50$. Parameters are: $\hat{u} = 0.15, \eta = 1.7, a = 0.25, \beta = 4$ and $\bar{u} = -0.954$.

physiologically realistic [1, 26, 38] gap junction conductance of $\gamma_c = 127$ pS, using the transformation resulting from nondimensionalization, $g_c = \gamma_c \bar{\tau}_n / C_m$, with $\bar{\tau}_n = 4.86$ ms (time scale of K^+ channel activation) and $C_m = 6158$ fF (cell capacitance) [28]. In this case, the last active cell is at $i = 50$, meaning that the waves propagate far into the region of cells that are silent in the absence of coupling (Fig. 1, bottom panel).

2.1 One-parameter bifurcation analysis

We now aim to understand why the waves propagate far into the region of "silent" cells. Intuitively, an otherwise silent cell is "pulled" into activity when its neighbor activates. To understand when and why this happens, we start out by analyzing the single cell model. Then, we investigate how the single-cell model structure is perturbed when one neighbor is active and the other is silent, which allows us to predict how far the wave will propagate.

2.1.1 Uncoupled single-cell bifurcation analysis

In [27], a detailed analysis of the single-cell model, i.e., (2) with $g_c = b_i = 0$, was made. This analysis uses a standard fast-slow approach [31] by setting $\epsilon = 0$ and performing a bifurcation analysis of the fast subsystem $(\dot{u}, u)$, i.e., the second order differential equation,

$$\ddot{u} + F(u)\dot{u} + G(u; c) = 0, \tag{4}$$

is analyzed assuming c constant.

The fixed points of the fast subsystem (4) lie along the cubic curve $G(u, c) = 0$ in the (c, u) plane, denoted the Z-curve (Fig. 2). This curve has a right knee at the point $K_\rho = (u_\rho, c_\rho) = (1, 5)$ and a left knee at $K_\lambda = (u_\lambda, c_\lambda) = (-1, 1)$. The Z-curve has upper, middle and lower branches Z_U, Z_M and Z_L defined for u in $(u_\rho, +\infty)$, (u_λ, u_ρ) and $(-\infty, u_\lambda)$, respectively. The region between c_λ and c_ρ is referred to as the region of multiple steady states (of the fast subsystem). With parameters as in Fig. 1, the critical points on Z_L, Z_M and Z_U are stable, saddles and stable/unstable spirals, respectively. A supercritical Hopf bifurcation (HB) arises on Z_U to the left of the left knee K_λ, giving rise to a branch of stable periodics that terminates in a homoclinic bifurcation (HC) on Z_M to the right of the left knee.

Square-wave bursting occurs [31] when the c-nullcline intersects the Z-curve on Z_M to the left of the HC, as for the cell $i = 1$ in Fig. 2. The system moves left along Z_L until in reaches K_λ where it rapidly shoots upwards to the stable periodic of the fast subsystem. Being above the c-nullcline, the system now moves towards the right along the branch of periodics, which produces the spikes of the active phase. When the system encounters the HC of the fast subsystem, the active phase terminates and the system rapidly tends to the stable fixpoint of the fast subsystem, which has reappeared, to begin the silent phase of bursting, and repeat the described events. When the c-nullcline intersects Z_L (e.g., cell 60 in Fig. 2), the point of intersection is a stable fixpoint for the full system $(u, \dot{u}, c)$, so that the cell is silent (in the absence of coupling). Thus, active and silent cells can be distinguished based on where their c-nullclines intersect the Z-curve. As it turns out from Fig. 1, top panel, and confirmed by Fig. 2, right panel, for the uncoupled cells, the first twenty-four cells are active while the remaining cells ($i \geq 25$) are silent.

2.1.2 Single-cell bifurcation analysis in presence of coupling

We now consider the fast subsystem version of (2) for coupled cells. We make the simplifying assumption that the membrane potentials of the cells neighboring cell i are constant, $u_{i-1} = u_H$ and $u_{i+1} = u_L$, with u_H equal to the maximum value of the membrane potential during bursting in the presence of coupling ($u_H = 1.5$), and u_L the value of the membrane potential of the lower SN ($u_L = -1$). The rational is that to investigate whether a silent cell (i) activates when the excitation wave arrives and activates the neighboring cell ($i - 1$), the most depolarized membrane potential of this cell should matter,

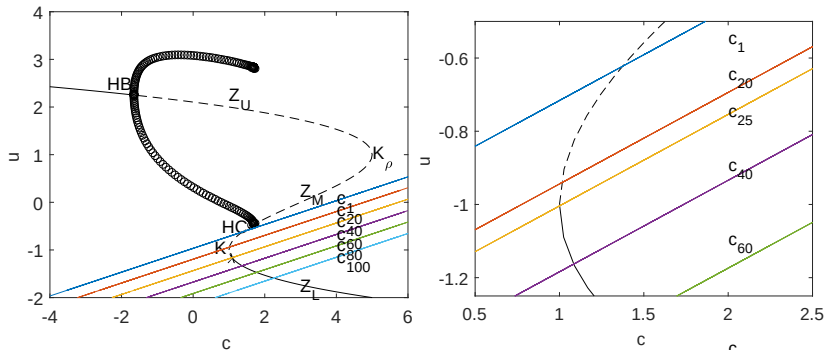

Fig. 2: Bifurcation diagram (black) of the fast subsystem (4), with six different c-nullclines superimposed (colored, indicated by c_i for the ith cell) corresponding to the cells in Fig. 1. The fix points fall on the cubic Z-curve, which is divided into its upper (Z_U), middle (Z_M), and lower (Z_L) branches, with right (K_ρ) and left (K_λ) knees. A supercritical HB arises on Z_U and an HC on Z_M. The black solid and dashed lines indicate stable and unstable equilibrium points, respectively, while the circles show maxima and minima of the stable periodics. The right panel shows a zoom on the region near K_λ. Notice that for $i \geq 25$, but not for $i \leq 24$, the c-nullcline intersects Z_L, and hence, cell no. 25 is the first silent cell. Parameters as in Fig. 1.

whereas the membrane potential of the silent neighbor (cell no. $i+1$ with $u_{i+1} = u_L$) may prevent the activation of cell i. These assumptions reduce the fast subsystem for cell i to

$$\ddot{u}_i + \tilde{F}(u_i)\dot{u}_i + \tilde{G}(u_i; c) = 0 \tag{5}$$

with

$$\tilde{F}(u_i) = F(u_i) + 2g_c \quad \text{and} \quad \tilde{G}(u_i; c) = G(u_i, c) + 2g_c u_i - g_c(u_H + u_L).$$

Notice that the changes in $\tilde{F}$ and $\tilde{G}$ due to coupling ($g_c > 0$) will modify the shape of the Z-curve (Fig. 3). For increasing g_c, the right knee K_ρ moves down and leftwards, while the left one, K_λ, moves upwards and to the right. Concerning the number of HB, increasing g_c from 0 to 0.05 gives rise to a second supercritical HB on Z_U (not shown), whereas no HBs are present on the Z-curve for $g_c = 0.1$, 0.2 or 0.5 (Fig. 3).

To understand how coupling changes otherwise silent cells, the location of K_λ matters. For example, cell no. 40 is silent in the absence of coupling since its nullcline intersect Z_L in this case (Fig. 2), say at (c^*_{40}, u^*_{40}). In the presence of coupling, e.g. $g_c = 0.1$ as in Fig. 1, if the neighboring cell activates so that $u_{39} \approx u_H$ even briefly, then cell no. 40 would experience that K_λ moves to the right of c_{40}. Since the dynamics of u is much faster than of c, the cell would shoot up and approach Z_U, i.e., the cell would activate.

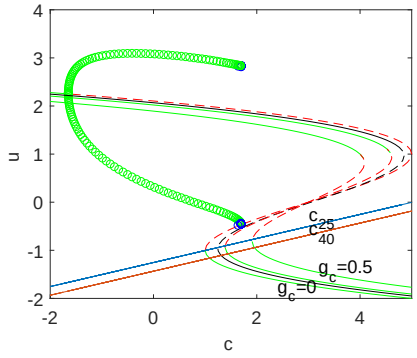

Fig. 3: Four different bifurcation diagrams of the fast subsystem of the Pernarowski model (5) for different values of g_c. Following Z_L from the bottom to the top, we have the bifurcation diagrams for $g_c = 0$, $g_c = 0.1$ (black), $g_c = 0.2$ and $g_c = 0.5$. Superimposed on the plot is the c-nullcline of the first silent cell when $g_c = 0$, c_{25}, and another silent cell (c_{40}) discussed in the main text. Legends as in Fig. 2. For $g_c = 0$ there is a supercritical HB on Z_U while for $g_c = 0.1$, $g_c = 0.2$ and $g_c = 0.5$ there are no HBs.

This mechanism is shown from another point of view in the phase-plane plots in Fig. 4 for the fast subsystem (5). Before the wave arrives, cell no. i and its two neighbors are all silent, i.e., the coupling term is zero (which can be obtained by setting $g_c = 0$ in (5)), and the system is located at the left, stable fix point, say $(u_0^*, 0)$, which depends on the c-value of cell i, c_i (Fig. 4a,b, square). When the wave arrives (modeled by $g_c > 0$ in (5)), cell i follows the curve in the phase plane with initial value $(u_0^*, 0)$ with virtually no change in c_i. The cell will remain silent if the lower equilibrium persists (Fig. 4c), whereas cell i will activate and approach the right equilibrium at $u \approx 2$ if, for a certain fixed c_i, a saddle-node bifurcation occurs as the coupling strength is raised from $g_c = 0$ so that the left equilibrium and the saddle disappear (Fig. 4d).

2.1.3 Two-parameters bifurcation analysis in the presence of coupling

From the above considerations it emerges that it is the location, in the absence of coupling, of the "silent cell" intersection between Z_L and the specific c-nullcline, say (c_i^*, u_i^*), compared to the location of the fast-subsystem saddle-node bifurcation (SN) occurring at K_λ, with coupling, that determines whether cell i is activated for a certain coupling strength g_c. If c_i^* is to the right of K_λ for a given g_c, then cell i will remain silent, otherwise it will become active and contribute to wave propagation.

We therefore constructed a two-parameters bifurcation diagram for the fast subsystem (5) with c and g_c as parameters (Fig. 5). In particular we plot the curve of the SN points, which confirms that the left SN (K_λ) moves to the

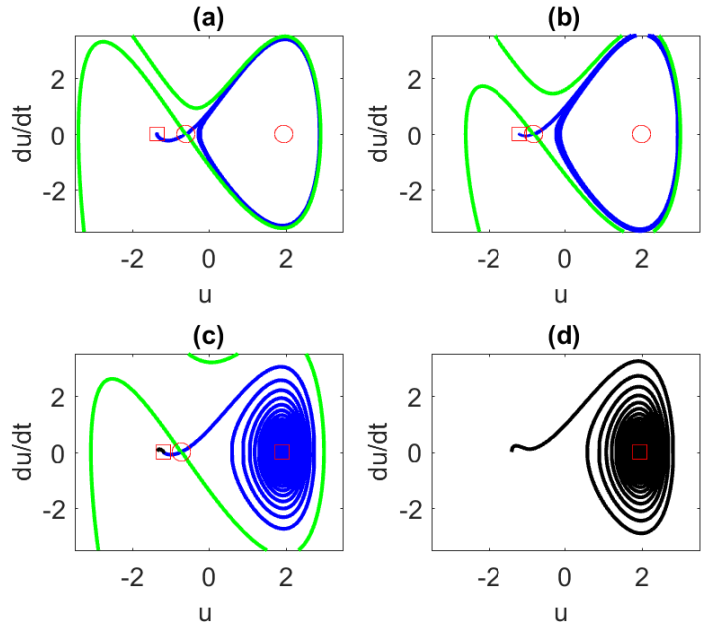

Fig. 4: Phase plane for the Pernarowski model (5) with $c = 1.4$ (panels (a) and (c)) or $c = 1.1$ ((b) and (d)), in the absence ($g_c = 0$; (a) and (b)) or presence ($g_c = 0.1$; (c) and (d)) of coupling. Stable fix points are represented with red squares and the unstable equilibria with red circles. The green (respectively, blue) lines depict the stable (respectively, unstable) manifolds of the saddle node points. The black lines show the trajectories with initial conditions equal to the stable fix point in the absence of coupling.

right as g_c increases, whereas K_ρ moves to the left. We performed simulations as in Fig. 1 for different coupling strengths, and extracted, for the first cell that remained silent for a given value of g_c, the c-value in the absence of coupling (denoted c^*), corresponding to c_i^* in the reasoning above. We then plotted (c^*, g_c) for each of the simulations (Fig. 5). These points fell very close to the SN curve, which confirmed that the location of the SN predicts how far into the silent region the wave will propagate, since cells that do not activate (right-most cells in Fig. 1), for a given g_c value, have higher c values (in the absence of coupling) than the extracted points c^* values and, hence, the c coordinate of the SN.

Since the SN moves to the right as g_c increases, this analysis indicate why waves always proceed substantially into the silent region. This holds true for any single-cell model where the silent phase terminates in a SN of a Z-shaped curve, which is the case for, to our knowledge, all published β-cell models.

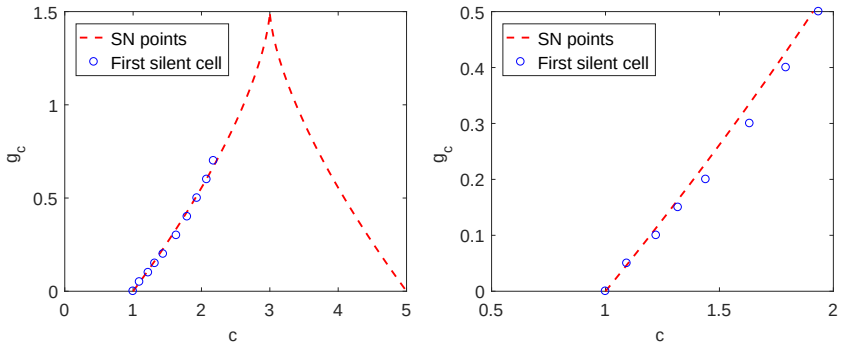

Fig. 5: Two-parameters bifurcation diagram for (c, g_c). The dashed red curve shows the location of SN points, whereas the blue circles indicate the first silent cell in simulations as in Fig. 1 for increasing values of g_c. The right panel is a zoom of the left panel.

3 The modified Pernarowski model

We speculated that it would be possible to avoid waves propagating into the silent region if the silent phase ended in another bifurcation than the SN at the left knee. One possibility could be that, for c decreasing, the fixed points on Z_L lost stability due to the presence of a subcritical HB on Z_L, which would terminate the silent phase.

The Pernarowski model for a single cell can be modified in such a way to have two HBs with different stability of the emerging periodics. In particular we wish to have a first supercritical HB on Z_U to the left of the left knee, K_λ, and a second subcritical HB on Z_L to the right of the left knee. This can be done changing the degree of $F(u)$ and generalizing $G(u, c)$ in the Pernarowski model. Let

$$\begin{aligned} S(u) &= a\left[(u-\hat{u})^6 - \eta^6\right], \\ T(u,c) &= c + u^3 - h(u+1), \end{aligned} \tag{6}$$

where S and T correspond to F and G, so that the model becomes

$$\ddot{u} + S(u)\dot{u} + T(u,c) = -\epsilon H(u,c), \qquad \dot{c} = \epsilon H(u,c). \tag{7}$$

As for the fast subsystem (4), the fixed points of the fast subsystem

$$\ddot{u} + S(u)\dot{u} + T(u;c) = 0, \tag{8}$$

lie along the curve $T = 0$, which is a cubic in the (c, u) plane that we denote the ζ-curve. It is composed of upper, middle and lower branches denoted ζ_U, ζ_M and ζ_L as for the Z-curve.

A fixed point is a Hopf point if the Jacobian matrix of (8) evaluated at that point has a simple pair of purely imaginary eigenvalues, that is, when the

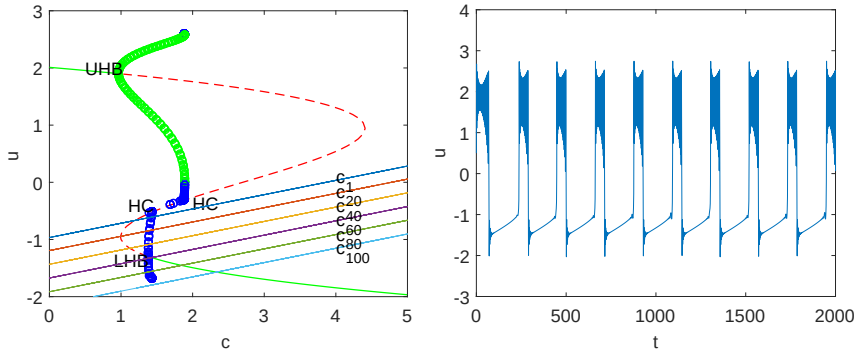

Fig. 6: Left: Bifurcation diagram of the fast subsystem (8). A supercritical HB arises on ζ_U and a subcritical one on ζ_L. Green solid line indicate stable equilibrium points while the dashed red line unstable ones. Six c nullclines, corresponding to an excitation gradient, are shown. To facilitate comparison between the Pernarowski model and the modified version, we chose the same values of $b_i = 0.012 \cdot i$ as in Fig. 1. Right: The membrane potential of the first cell in time for the modified Pernarowski model (7).

determinant of the matrix is positive and the trace is zero, which yield

$$\begin{aligned} T(u;c) &= 0, \\ T_u(u;c) = 3u^2 - h &> 0, \\ S(u) &= 0. \end{aligned} \tag{9}$$

Despite S being a sixth order polynomial in u, it has only two real roots, the same as for F in the Pernarowski model, $u_\pm = \hat{u} \pm \eta$. The stability of the periodic orbits emanating from the Hopf point u_+ is determined by the sign of (compare with [27])

$$a_{HB+} = 18a\eta^4 \left(-8\eta\hat{u} - 3\eta^2 - 5\hat{u}^2 + \frac{5h}{3} \right),$$

and at the HB point u_- by the sign of

$$a_{HB-} = 18a\eta^4 \left(8\eta\hat{u} - 3\eta^2 - 5\hat{u}^2 + \frac{5h}{3} \right).$$

Based on these consideration we choose the following set of parameters,

$$\hat{u} = 0.3, \quad \eta = 1.6, \quad a = 0.025, \quad \beta = 4, \quad h = 2.7, \quad \bar{u} = -0.954, \tag{10}$$

and construct the bifurcation diagram of the fast subsystem (8) (Fig. 6, left). As desired, a supercritical HB (UHB) arises on ζ_U to the left of the left knee, and a subcritical one (LHB) arise on ζ_L to the right of the left knee, and the system (7) exhibits square-wave bursting (Fig. 6, right).

Let us consider a model for a chain of coupled cells with an excitation gradient (modeled via b_i) as in Section 2,

$$\begin{aligned}\ddot{u}_i + [S(u_i) + 2g_c]\,\dot{u}_i + [T(u_i, c) + 2g_c u_i] \\ - g_c(u_{i+1} + u_{i-1} + \dot{u}_{i+1} + \dot{u}_{i-1}) = -\epsilon H(u_i, c), \\ \dot{c}_i = \epsilon H(u_i, c_i). \quad (11)\end{aligned}$$

Due to the excitation gradient, for $g_c = 0$ the last active cell is at $i = 55$ (Fig. 7, top). This corresponds to the fact that the intersection between the c-nullcline and the lower branch of the ζ-curve (ζ_L) occurs to the right of LHB for $i > 55$, whereas the intersection lies on ζ_M, or on ζ_L to the left of LHB, otherwise (Fig. 6, left). In contrast to Fig. 1, with coupling ($g_c = 0.1$) the wave does not propagate far into the "silent" region, but stops approximately at the border between the active and silent regions at cell $i = 59$ (Fig. 7, bottom).

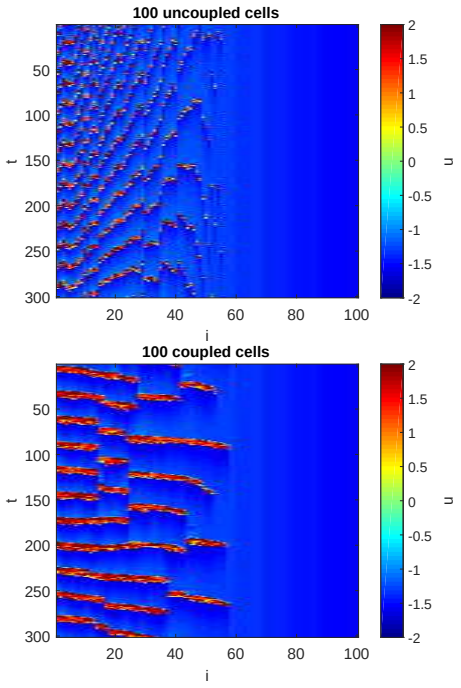

Fig. 7: Simulations with the modified model in an excitation gradient. Top: 100 uncoupled cells, $g_c = 0$, were simulated and the last active cell is for $i = 55$. Bottom: For 100 coupled cells, $g_c = 0.1$, the last active cell is for $i = 59$. u is the membrane potential, t time and i the cell counter. $b_i = 0.012 \cdot i$ as in Figs. 1 and 6.

3.1 One-parameter bifurcation analysis

To better understand why the wave propagation behaves differently in the Pernarowski model and our modified version, we proceed as in Section 2.1.2. We consider the membrane potential u_i of cell no. i, and assume that the membrane potentials of the neighbor cells are constant, $u_{i-1} = u_H$ and $u_{i+1} = u_L$, with $u_H = 1.559$ the action potential peak value, and $u_L = -1.3$ the membrane potential value at LHB. These assumptions yield the fast subsystem version of (11) in the form

$$\ddot{u}_i + \tilde{S}(u_i)\dot{u}_i + \tilde{T}(u_i; c) = 0 \tag{12}$$

with

$$\tilde{S}(u_i) = S(u_i) + 2g_c \quad \text{and} \quad \tilde{T}(u_i; c) = T(u_i; c) + 2g_c u_i - g_c(u_H + u_L).$$

Solving the equation $\tilde{S}(u_i) = 0$ we get the analytical expression of the two HB points as was made for one cell, $\tilde{u}_\pm = \hat{u} \pm \tilde{\eta}$, with $\tilde{\eta} = (\eta^6 - 2g_c/a)^{1/6}$. Thus the LHB, which terminates the silent phase, moves (slightly) to the left as g_c increases, in contrast to the SN terminating the silent phase in the original model, which moved to the right (Fig. 5).

In Fig. 8, the bifurcation diagram of the fast subsystem (12) is plotted for different values of g_c. The ζ-curve change similarly to the Z-curve as g_c increases; the right knee moves in down-left direction while the left knee moves upwards and to the right. For $g_c = 0$ and $g_c = 0.1$ there are two HBs (a supercritical one on ζ_U and an subcritical one on ζ_L), whereas for $g_c = 0.2$ only the HB on ζ_U is present, and finally for $g_c = 0.5$ no HB remains.

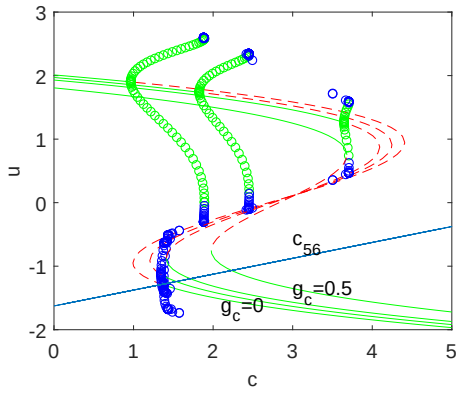

Fig. 8: Four bifurcation diagrams of the fast subsystem of modified Pernarowski model (12) for different values of g_c. Looking at ζ_L from the bottom to the top we have the bifurcation diagrams for $g_c = 0$, $g_c = 0.1$, $g_c = 0.2$ and $g_c = 0.5$. Superimposed on the plot is the c-nullcline of the first silent cell when $g_c = 0$, c_{56}.

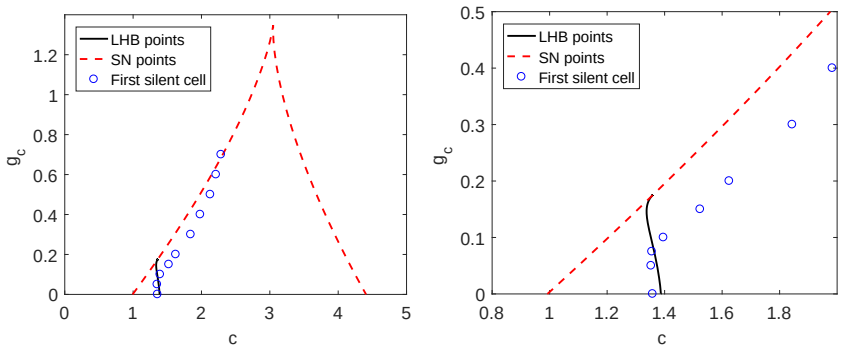

Fig. 9: Two-parameter bifurcation diagram for (c, g_c). The blue circles indicate the c values in the absence of coupling for the first silent cell in simulations as in Fig. 7 with varying coupling strength g_c. The right panel is a zoom of the left panel.

3.2 Two-parameters bifurcation analysis

As for the Pernarowski model (5), we constructed the two-parameter bifurcation diagram for the modified model (12) with c and g_c as bifurcation parameters (Fig. 9). As for the original model, the SN at the left knee moves to the right as g_c increases, but – more important – for low g_c values, the LHB moves to the left as g_c increases, until the LHB branch disappears in a Bogdanov-Takens bifurcation at $g_c \approx 0.19$. Since the silent phase ends at the LHB, the prediction is that the wave should stop earlier with low to moderate coupling compared to the case without coupling. Direct simulations confirm this prediction for $g_c = 0.05$ where the last active cell is no. 54, whereas the last active cell is no. 55 with $g_c = 0$ (Fig. 7, upper). For higher values of g_c it is the SN that ends the silent phase, and the waves are predicted to proceed into the silent region as for the Pernarowski model. However, the simulated waves proceed further than predicted from the SN curve (Fig. 9).

To understand why the location of the SN bifurcation fails to predict exactly where the waves stop, we construct phase planes for the fast subsystem of the modified model (12). In Fig. 10 we investigate the case $g_c = 0.2$ for two c-values where the saddle node exists, i.e., c-values to the right of the SN (red, dashed curve in Fig. 9). For $c = 1.7$, the scenario is as expected: the left, stable equilibrium exists also when the cells are coupled, and the trajectory starting from the location of the left fix point in the absence of coupling (square in Fig. 10a) approaches this left equilibrium also in the presence of coupling (Fig. 10c), meaning that the cell would remain silent should the wave arrive and activate its neighbor. In contrast, for $c = 1.5$ the stable left equilibrium exists also in the presence of coupling, but now the location of the equilibrium in the absence of coupling (square in Fig. 10b) falls to the left of the stable manifold of the saddle node so that the trajectory escapes and approaches the right equilibrium (Fig. 10d), i.e., the cell activates and contributes to wave

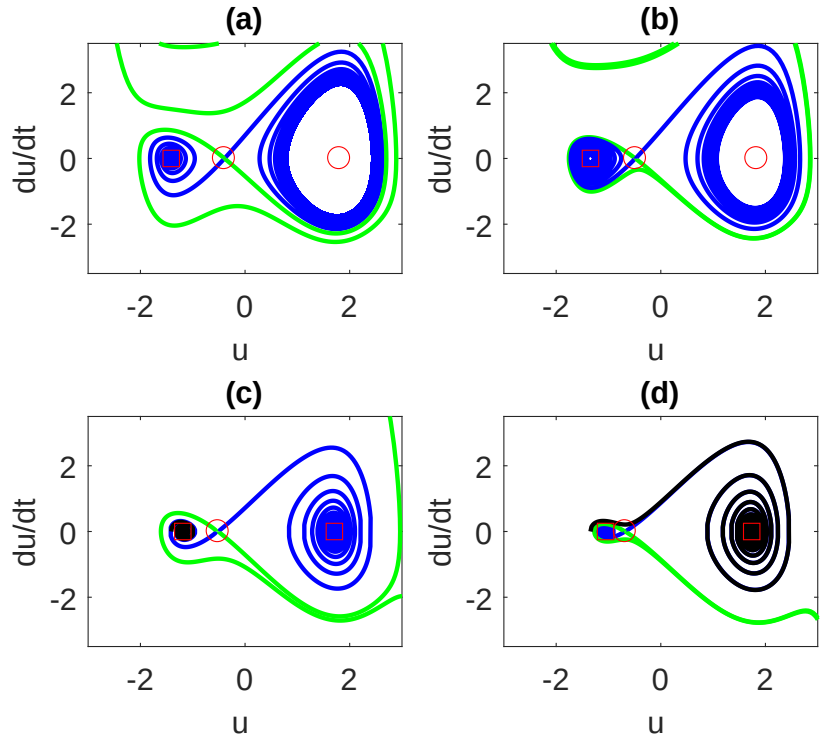

Fig. 10: Phase plane for the modified Pernarowski model (12) with $c = 1.7$ (panels (a) and (c)) or $c = 1.5$ ((b) and (d)), in the absence ($g_c = 0$; (a) and (b)) or presence ($g_c = 0.2$; (c) and (d)) of coupling. Stable fix points are represented with red squares and the unstable equilibria with red circles. The green (respectively, blue) lines depict the stable (respectively, unstable) manifolds of the saddle node points. The black lines show the trajectories with initial conditions equal to the stable fix point in the absence of coupling.

propagation. Thus, the fact that the stable left equilibrium exists does not suffice to keep the cell silent; it depends on whether the left equilibrium in the absence of coupling falls outside the separatrix, which wraps tightly around the left equilibrium in the modified model (Fig. 10) compared to the original Pernarowski model (Fig. 4). These considerations explain why the waves propagate further than predicted by the SN curve (Fig. 9).

4 Cubic cluster of cells

Until now we have considered a line of coupled cells. Pancreatic islets are three-dimensional structures, so we simulate a $8 \times 8 \times 8$ cell cluster to verify that the differences, with respect to wave stop, between Pernarowski's model and the modified version introduced in this paper carry over to this case.

When the single cells were represented by Pernarowski's model, and an excitation gradient was imposed by setting $b_i = 0.05 \cdot (1 + i)$ for all 64 cells in slice $i = 1, \ldots, 8$, only the first four slices are active while the last ones are silent in the uncoupled case $g_c = 0$ (Fig. 11a). In contrast, with $g_c = 0.1$, all the cells of the cube became active (Fig. 11b), i.e., the wave did not stop.

Similar simulations were performed for the modified model with $b_i = 0.4 + 0.05 \cdot (1+i)$. For uncoupled cells, the first four slices of cells are active while the remaining ones are not (Fig. 11c). For coupled cells ($g_c = 0.1$), the waves do not proceed beyond the fourth slice (Fig. 11d). Thus, for the modified version of Pernarowski's model, we have that also for a cube of coupled β-cells, the wave stops at the border between silent and active cells, as seen in experiments.

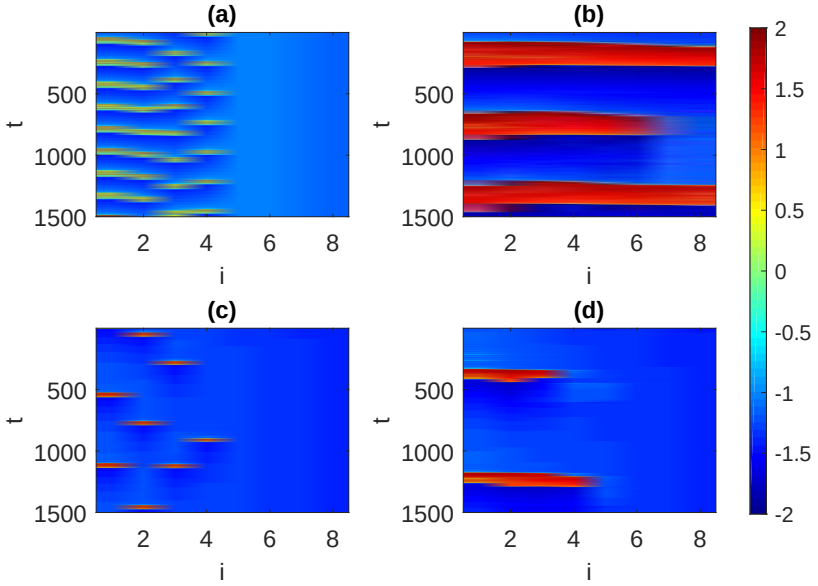

Fig. 11: Cluster of $8 \times 8 \times 8$ β-cells modelled by Pernarowski's model (2) (panels (a) and (b)), or our modified version (11) ((c) and (d)), in the absence ($g_c = 0$; (a) and (c)) or presence ($g_c = 0.1$; (b) and (d)) of gap junction coupling. Each panel shows the membrane potential for a cell in each of the eight slices ($i = 1, \ldots, 8$) of the cube vs. time t. Within each slice, the activity is synchronized.

5 Discussion

Mathematical modeling is increasingly used to study phenomena such as wave propagation and synchrony in biological ensembles. Previously published models of bursting β-cells have successfully given insight into cellular mechanisms,

and to some extent into the behavior of the population of electrically coupled cells in pancreatic islet. However, to the best of our knowledge, all existing models tend to synchronize too easily compared to biological results. In particular, the experimentally observed wave stop at the border between "silent" and "active" cells in islets exposed to a glucose gradient [5, 33], for the particular case of β-cell can only be reproduced in simulations by imposing unrealistic assumptions regarding islet organization, coupling strength, or cellular heterogeneity [3, 5, 11, 19, 25].

Inspired by the example of pancreatic β-cells, we set out to study synchronization and wave properties of general coupled square-wave bursters. Using fast-slow bifurcation analysis, we clarified why waves tend to propagate too far into the silent region as shown in our simulations (Fig. 1). We showed that the left saddle-node bifurcation (SN) moves to right in the presence of coupling, and that the location of this bifurcation predicts where the simulated waves stop (Fig. 5). Since square-wave bursting models have in common that the silent phase is terminated as the system reaches the SN bifurcation, this result (i) explains why they fail in reproducing the wave behavior in islets exposed to an excitation gradient, and (ii) suggests that the models should end the silent phase in another way in order to reproduce this experimental behavior.

We modified the Pernarowski model to get a Hopf bifurcation (HB) of the lower branch of the ζ-curve, so that the silent phase terminates due to this HB (Fig. 6), and showed that with realistic coupling strength, and in the absence of cellular or coupling heterogeneity, this modified model produces waves that stop at the border between active and silent cells, both in 1D (Fig. 7) and 3D (Fig. 11) lattice configurations.

The bifurcation analysis of the modified model led to an underestimate of how far the waves would propagate (Fig. 9). We showed that this modest error was due to the way the separatrix wraps tightly around the left equilibrium in this model (Fig. 10).

We analyzed a prototypical model with only one slow and two fast variables. Of interest, it has been found that a more complicated so-called phantom burster model with two slow (and two fast) variables, of which one variable is much slower than the other, can have a Hopf bifurcation on the lower branch when the slowest variable is used as a bifurcation parameter in the three-dimensional fast subsystem [8]. In [9] we have investigated the criteria for obtaining the scenario by studying a "phantom" version of the Pernarowski model, which should help in obtaining the correct geometrical structure of future biophysical models.

Although our model analysis was inspired by data and models of pancreatic β-cells, we do not claim that our modified model with lower Hopf bifurcation is the correct or only way to improve current β-cell models. Rather, our aim was to show how slow-fast analysis can be used to predict wave block in a general population of square-wave bursters.

Acknowledgements This work was supported by the University of Padova, Strategic Research Project "DYCENDI", and Research Project SID (BIRD179302), to M.G.P. The re-

search of I.M.B. has been partially supported by Finanziamento GNCS Giovani Ricercatori 2018/2019

Conflict of interest The authors declare that they have no conflict of interest.

References

1. Andreu E, Bernat S, Sanchez-Andres JV (1997) Oscillation of gap junction electrical coupling in the mouse pancreatic islets of Langerhans. J Physiol 498:753–761
2. Aslanidi OV, Mornev O, Skyggebjerg O, Arkhammar P, Thastrup O, Sørensen M, Christiansen P, Conradsen K, Scott A (2001) Excitation wave propagation as a possible mechanism for signal transmission in pancreatic islets of Langerhans. Biophys J 80:1195–1209
3. Barua AK, Goel P (2016) Isles within islets: The lattice origin of small-world networks in pancreatic tissues. Physica D: Nonlinear Phenomena 315:49–57
4. Benninger RKP, Zhang M, Head WS, Satin LS, Piston DW (2008) Gap junction coupling and calcium waves in the pancreatic islet. Biophys J 95(11):5048–61, DOI 10.1529/biophysj.108.140863
5. Benninger RKP, Hutchens T, Head WS, McCaughey MJ, Zhang M, Le Marchand SJ, Satin LS, Piston DW (2014) Intrinsic islet heterogeneity and gap junction coupling determine spatiotemporal Ca^{2+} wave dynamics. Biophys J 107(11):2723–33, DOI 10.1016/j.bpj.2014.10.048
6. Bernstein SA, Morley GE (2006) Gap junctions and propagation of the cardiac action potential. Adv Cardiol 42:71–85, DOI 10.1159/000092563
7. Bertram R, Sherman A, Satin LS (2007) Metabolic and electrical oscillations: partners in controlling pulsatile insulin secretion. Am J Physiol Endocrinol Metab 293(4):E890–E900, DOI 10.1152/ajpendo.00359.2007
8. Bertram R, Rhoads J, Cimbora WP (2008) A phantom bursting mechanism for episodic bursting. Bull Math Biol 70(7):1979–93, DOI 10.1007/s11538-008-9335-0
9. Bulai IM, Pedersen MG (2018) Hopf bifurcation analysis of the fast subsystem of a polynomial phantom burster model. Dolomites Research Notes on Approximation, 11(3):3–10, DOI 10.14658/pupj-drna-2018-3-2
10. Butera RJ Jr, Rinzel J, Smith JC (1999) Models of respiratory rhythm generation in the pre-bötzinger complex. I. bursting pacemaker neurons. J Neurophysiol 82(1):382–97
11. Cappon G, Pedersen MG (2016) Heterogeneity and nearest-neighbor coupling can explain small-worldness and wave properties in pancreatic islets. Chaos 26(5):053103, DOI 10.1063/1.4949020
12. Chay TR, Keizer J (1983) Minimal model for membrane oscillations in the pancreatic beta-cell. Biophys J 42(2):181–190, DOI 10.1016/S0006-3495(83)84384-7

13. De Vries G, Sherman A (2000) Channel sharing in pancreatic beta - cells revisited: enhancement of emergent bursting by noise. J Theor Biol 207(4):513–30, DOI 10.1006/jtbi.2000.2193
14. De Vries G, Sherman A (2001) From spikers to bursters via coupling: help from heterogeneity. Bull Math Biol 63(2):371–391, DOI 10.1006/bulm.2001.0228
15. De Vries G, Sherman A, Zhu HR (1998) Diffusively coupled bursters: effects of cell heterogeneity. Bull Math Biol 60(6):1167–200
16. Dolenšek J, Stožer A, Skelin Klemen M, Miller EW, Slak Rupnik M (2013) The relationship between membrane potential and calcium dynamics in glucose-stimulated beta cell syncytium in acute mouse pancreas tissue slices. PLoS One 8(12):e82374, DOI 10.1371/journal.pone.0082374
17. Hindmarsh JL, Rose RM (1984) A model of neuronal bursting using three coupled first order differential equations. Proc R Soc Lond B Biol Sci 221(1222):87–102
18. Loppini A, Pedersen MG (2018) Gap-junction coupling can prolong beta-cell burst period by an order of magnitude via phantom bursting. Chaos 28(6):063111, DOI 10.1063/1.5022217
19. Meyer-Hermann M, Benninger RKP (2010) A mathematical model of β-cells in an islet of Langerhans sensing a glucose gradient. HFSP J 4(2):61–71, DOI 10.2976/1.3354862
20. Pedersen MG (2004) Homogenization of heterogeneously coupled bistable ode's-applied to excitation waves in pancreatic islets of Langerhans. J Biol Phys 30(3):285–303, DOI 10.1023/B:JOBP.0000046727.28337.f4
21. Pedersen MG (2005) A comment on noise enhanced bursting in pancreatic beta-cells. J Theor Biol 235(1):1–3, DOI 10.1016/j.jtbi.2005.01.025
22. Pedersen MG (2005) Wave speeds of density dependent Nagumo diffusion equations–inspired by oscillating gap-junction conductance in the islets of Langerhans. J Math Biol 50(6):683–98, DOI 10.1007/s00285-004-0304-4
23. Pedersen MG (2009) Contributions of mathematical modeling of beta cells to the understanding of beta-cell oscillations and insulin secretion. J Diabetes Sci Technol 3(1):12–20
24. Pedersen MG (2010) A biophysical model of electrical activity in human β-cells. Biophys J 99(10):3200–3207, DOI 10.1016/j.bpj.2010.09.004
25. Pedersen MG, Sørensen MP (2008) Wave-block due to a threshold gradient underlies limited coordination in pancreatic islets. J Biol Phys 34(3-4):425–32, DOI 10.1007/s10867-008-9069-0
26. Pérez-Armendariz M, Roy C, Spray DC, Bennett MV (1991) Biophysical properties of gap junctions between freshly dispersed pairs of mouse pancreatic beta cells. Biophys J 59(1):76–92, DOI 10.1016/S0006-3495(91)82200-7
27. Pernarowski M (1994) Fast subsystem bifurcations in a slowly varying Liénard system exhibiting bursting. SIAM J Appl Math 54:814–832
28. Pernarowski M (1998) Fast and slow subsystems for a continuum model of bursting activity in the pancreatic islet. SIAM Journal on applied mathematics 58(5):1667–1687

29. Pernarowski M, Miura RM, Kevorkian J (1991) The Sherman-Rinzel-Keizer model for bursting electrical activity in the pancreatic β-cell. In: Differential Equations Models in Biology, Epidemiology and Ecology, Springer, pp 34–53
30. Pernarowski M, Miura R, Kevorkian J (1992) Perturbation techniques for models of bursting electrical activity in pancreatic β-cells. SIAM J Appl Math 52:1627–1650
31. Rinzel J (1985) Bursting oscillations in an excitable membrane model. In: Sleeman B, Jarvis R (eds) Ordinary and Partial Differential Equations, Springer-Verlag, New York, pp 304–316
32. Riz M, Braun M, Pedersen MG (2014) Mathematical modeling of heterogeneous electrophysiological responses in human β-cells. PLoS Comput Biol 10(1):e1003389, DOI 10.1371/journal.pcbi.1003389
33. Rocheleau JV, Walker GM, Head WS, McGuinness OP, Piston DW (2004) Microfluidic glucose stimulation reveals limited coordination of intracellular Ca^{2+} activity oscillations in pancreatic islets. Proc Natl Acad Sci 101:12899–12903
34. Rorsman P, Eliasson L, Kanno T, Zhang Q, Gopel S (2011) Electrophysiology of pancreatic β-cells in intact mouse islets of Langerhans. Prog Biophys Mol Biol 107(2):224–35, DOI 10.1016/j.pbiomolbio.2011.06.009
35. Shilnikov A, Kolomiets M (2008) Methods of the qualitative theory for the Hindmarsh–Rose model: A case study–a tutorial. International Journal of Bifurcation and chaos 18(08):2141–2168
36. Stožer A, Dolenšek J, Rupnik MS (2013) Glucose-stimulated calcium dynamics in islets of Langerhans in acute mouse pancreas tissue slices. PLoS One 8(1):e54638, DOI 10.1371/journal.pone.0054638
37. Tabak J, Toporikova N, Freeman ME, Bertram R (2007) Low dose of dopamine may stimulate prolactin secretion by increasing fast potassium currents. J Comput Neurosci 22(2):211–22, DOI 10.1007/s10827-006-0008-4
38. Zhang Q, Galvanovskis J, Abdulkader F, Partridge CJ, Göpel SO, Eliasson L, Rorsman P (2008) Cell coupling in mouse pancreatic beta-cells measured in intact islets of Langerhans. Philos Trans A Math Phys Eng Sci 366(1880):3503–23, DOI 10.1098/rsta.2008.0110